Applied Catalysis B: Environmental 185 (2016) 189–202

Contents lists available at ScienceDirect

Applied Catalysis B: Environmental

journal homepage: www.elsevier.com/locate/apcatb

Pd model catalysts: Effect of aging duration on lean redispersion

Jason A. Lupescu[a,b,*], Johannes W. Schwank[a], Galen B. Fisher[a], Xiaoyin Chen[a], Sabrina L. Peczonczyk[b], Andy R. Drews[b]

[a] University of Michigan, Ann Arbor, MI 48109 USA
[b] Ford Motor Company, Dearborn, MI 48124 USA

ARTICLE INFO

Article history:
Received 21 August 2015
Received in revised form 3 November 2015
Accepted 8 December 2015
Available online 10 December 2015

Keywords:
Palladium
Ceria–zirconia
Redispersion
TWC
Aging

ABSTRACT

An automotive three-way catalyst (TWC) deteriorates as a function of temperature, time and aging environment. While much effort has gone into formulating durable exhaust catalysts, relatively little attention has been paid to controlling the aging environment on the vehicle with techniques currently in use to protect the catalyst and counteract the increasing demands for higher fuel economy (e.g., overfueling to reduce exhaust temperatures). New engine control methods that are designed to minimize aging may be possible that can reduce the extent of catalyst deactivation and provide a lean environment capable of redispersing many of the precious metal particles. To develop improved engine control methods, detailed experimental information is needed to map the response of the catalyst to different aging conditions. In this report, we examine palladium-based model powder catalysts on ceria–zirconia, which were exposed to three different exhaust compositions, lean-only, rich-only and redox, each at 700 °C for three different durations, 20 min, 2 h and 16 h. Residual catalyst activity and metal-support interaction were probed with Water Gas Shift (WGS) reaction and Oxygen Storage Capacity (OSC) measurements. The Pd metal particle size and dispersion were estimated by H_2 chemisorption and XRD line broadening. Lean catalyst treatments at 550 °C and 700 °C were applied to determine the effect on Pd size and catalyst activity. An infrared study of CO adsorption onto the catalysts was used to identify whether Pd crystallite facets were covered by the support after exposure to the redox aging environment then again after the lean treatments were applied. The aging temperature and reducing gas environment significantly deteriorated catalytic activity through a combination of metal oxidation state effects and support interactions, while the aging duration was linked to the extent of Pd sintering reversibility through lean treatments. These insights provide a basis to develop engine control and aftertreatment design strategies to avoid severe aging modes and determine how often to actively intervene to regenerate the catalyst.

1. Introduction

The automotive catalytic converter, or Three-Way Catalyst (TWC), works in unison with engine controls that manage exhaust gas oxygen (O_2) concentration to abate regulated fuel combustion products like carbon monoxide (CO). The TWC washcoat contains a noble metal catalyst (i.e., Pd) impregnated onto a high surface area support material composed of alumina (Al_2O_3), oxygen storage capacity (OSC) promoters including mixtures of ceria and zirconia (CZO), and durability stabilizers such as rare earth oxides lanthana (La_2O_3) and yttria (Y_2O_3) [1]. The on-board engine control computer is essential to enable brief, controlled cycling of fuel-rich (oxygen deficient) and fuel-lean (excess oxygen) combustion exhaust to perform simultaneous oxidation and reduction reactions [1,2]. Over time, the TWC typically shows decreased efficiency of these reactions under the same exhaust environment, which is linked to deactivation. TWC deactivation modes include noble metal sintering [3,4], poisoning by fuel and oil additives [5], loss of surface area and OSC component sintering [1,2,6]. Characterization studies of full useful-life aged automotive TWCs revealed that the dispersion of noble metals had fallen to only about 1–5% [7,8], revealing that the vast initial amount of metal was buried inside large metal agglomerates and lost to involvement in gas-phase reactions. While in similar studies, OSC component sintering was explained by loss of contact between the noble metal and the OSC component [9–14], and by partial migration of OSC component materials, covering the noble metal [15–17].

Although TWC deactivation is largely irreversible, prolonged exposure to an oxidative gas environment can cause changes to

* Corresponding author at: Ford Motor Company, RIC Bldg MD 3179, P.O. Box 2053, Dearborn, MI 48121, USA.
E-mail address: jlupescu@ford.com (J.A. Lupescu).

http://dx.doi.org/10.1016/j.apcatb.2015.12.012
0926-3373/

the metal that result in partial reactivation. An increase in the Pd metal dispersion was observed following dry oxygen treatment that resulted in a lower temperature required for 50% conversion of combustion pollutants [18,19]. In another study, Pd particles on an Al_2O_3 support heated in a feed containing oxygen were observed to transform into PdO above 325 °C, and upon further heating from 350 °C to 800 °C the particles wet and spread over the support [20,21], ultimately shrinking to a size below the detection limit of the electron microscope used [22]. Pd redispersion is generally believed to begin at the temperature when Pd particles oxidize to PdO, and this temperature depends upon the Pd particle size [20,23]. PdO is stable up to 800 °C in air and does not sinter or emit adatoms [24]. This enables PdO to wet and spread over the support. The onset temperature of redispersion was found to decrease with increasing Pd metal dispersion (decreasing Pd crystal size) [20,23]. Pd redispersion is therefore thought to occur through the oxide form as it does not occur above the temperature of PdO decomposition [20,21], which is both a function of the support material and gas phase oxygen concentration [21,25,26]. To be of automotive relevance, intentional Pd redispersion would ideally be performed within the time scale of an engine deceleration fuel cut, which was shown to expose the catalyst to air for about 2–10 s on the FTP-75 (federal drive cycle) [27]. Newton et al. performed redox cycling at 400 °C with 2 wt% Pd/Al_2O_3 and observed that the Pd particle size immediately dropped from an average of 600 atoms per particle to about 20 atoms per particle within 2 s of the lean cycle onset, coinciding with the Pd to PdO transition [28]. If the Pd oxidation rate can be measured, then the Pd redispersion rate can be estimated and used as part of an engine control strategy to optimize the redispersion process.

The goal of this investigation was to determine how characteristics of deactivated model Pd catalysts aged for different durations were affected by exposure to post-aging oxidizing gas environments. Active intervention into the TWC aging process using periodic oxidative engine exhaust events may be useful to restore the catalyst conversion efficiency. However, the limits to the effectiveness of this regeneration method are unknown. To be fully effective, a detailed understanding of the Pd particle size response is needed. There is no one technique that can derive the true Pd size on CZO supports, so a synthesis of multiple, yet limited techniques, were used so that a consistent interpretation could be made. This requires evaluation of a TWC to characterize the Pd particle size in concert with probe reactions to assess the metal-support interface and measure residual catalyst activity, support surface area changes and PdO formation rate. While these evaluations may suggest a strong metal support interaction (SMSI) with Ce migrating and decorating the Pd surface during reducing conditions [15,29–32], obtaining direct evidence with high resolution electron microscopy is extremely difficult due to poor contrast between Pd, Zr and Ce. However, CO adsorption onto the surface of supported Pd catalysts during acquisition of infrared spectra has shown capability to identify the accessible Pd facets [33,34] and provide evidence of coverage via SMSI [30]. Here, we characterize these changes and identify the most severe deactivation modes so that they can be avoided through engine control methods.

2. Experimental

2.1. Preparation of model TWC samples

A model powder catalyst of 1.5 wt% Pd on ceria–zirconia (Pd/CZO) was prepared at a Ford OEM supplier laboratory by incipient-wetness impregnation of the ceria–zirconia ($Ce_{0.5}Zr_{0.5}O_2$) support with a palladium solution free from chlorides. After drying, this catalyst was calcined at 500 °C for 4 h in air to fix the Pd on the CZO material. Uncatalyzed ceria–zirconia ($Ce_{0.5}Zr_{0.5}O_2$) powder was also used as a standard to acquire baseline characterization data. The powders were then sieved to obtain particles between 40 and 60 mesh (250–420 microns).

2.2. TWC aging procedures

Catalyst aging environments were established in a continuous flow reactor at 700 °C with a tight air–fuel modulation to represent operating conditions of an automotive close-coupled catalytic converter. Three aging gas compositions were used: lean-only (0.1% O_2, 10% H_2O and N_2), rich-only (0.15% CO, 0.05% H_2, 10% H_2O and N_2) and redox conditions where the lean and rich feeds were alternated in 10 min step pulses. The CO gas stream was scrubbed of iron carbonyls. A round bottomed quartz boat measured 100 mm long, 17 mm wide and 5 mm tall was loaded with 1.50 g of catalyst powder and placed inside a 19 mm ID quartz reaction tube in the heating zone of the surrounding oven with a 1/16 inch diameter thermocouple placed over the boat in the aging gas stream and a 1/32 inch diameter thermocouple bent into the boat with the tip buried in the powder. Sample sets were aged for 20 min, 2 h and 16 h, respectively.

2.3. TWC preconditioning

Since gasoline engines operate close to stoichiometry, the catalyst OSC state is generally partly depleted. Therefore at the beginning of all characterization and activity measurements for this study, all samples were initially in a reduced state produced by exposure to 9% H_2 in argon at 300 °C for 30 min flowing at 0.22 L/min to remove all surface oxygen. The samples were then cooled in argon to room temperature.

2.4. TWC characterization techniques

The phase identification of the Pd/CZO catalysts was confirmed by X-ray diffraction (XRD) pattern analysis. A Rigaku Miniflex II diffractometer was used with a Cu Kα X-ray (λ = 1.5406 Å) radiation source set at 30 kV and 15 mA. A catalyst sample mass of 0.1 g was wet-milled with a mortar and pestle in ethanol then dripped onto an off-axis cut silicon crystal sample substrate and dried. Scans were performed with a step size of 0.005°2θ at a scan speed of 1°2θ/min from 5°2θ to 90°2θ.

The surface characteristics of the catalysts were determined by N_2 physisorption, X-ray photoelectron spectroscopy (XPS) and Diffuse Reflectance Infrared Fourier Transform Spectroscopy (DRIFTS). The BET specific surface area and BJH pore volume (for pores between 17 and 300 Å) were determined with a Micromeritics ASAP2420 instrument using N_2 adsorption at 77 K. A 48-point adsorption and 33-point desorption isotherm plot was generated across a range of 0.1–0.9 P/P_0. Elemental composition and chemical state information were determined with a Kratos AXIS 165 Electron Spectrometer using a monochromatic Al Kα (1486.6 eV) X-ray excitation source operated at 12 kV, 20 mA (240 W). Each sample was pressed into a pellet and then mounted onto sticky double sided pressure sensitive adhesive tape. Data were collected using pass energies of 80 eV or 20 eV to obtain survey or high resolution spectra, respectively. All spectra were acquired using charge neutralization with an electron flood source. Elemental quantification of the high resolution spectra was accomplished using CASAXPS software Version 2.3.16, using routines based on Scofield photoionization cross-section values. A Shirley type background was used to fit all high resolution spectra. The Zr 3p fit was first determined from a CZO standard using 60% Gaussian and 40% Lorentzian line shapes with an area ratio of 0.5, a full width at half maximum (FWHM) constrained between 0.6–2.8, and a peak separation of 13.4 eV. The

remaining area under the envelope was then fit by adding Pd 3d peaks. The Pd 3d species was fit with a doublet using 60% Gaussian and 40% Lorentzian line shapes with an area ratio of 0.667, a FWHM constrained within 0.6–2.8, and a peak separation of 5.2 eV. Binding energies were referenced to the aliphatic C 1s peak at 284.6 eV [35]. Infrared spectra were collected with a Nicolet 6700 FTIR spectrometer with Auxiliary Experiment Module including a praying mantis cell to facilitate gas exchange to and heating of the sample. Fine powder catalyst samples recovered from the XRD analysis were poured into the praying mantis sample cup onto a supporting screen. Clean samples were prepared as follows: (1) 25% H_2 in nitrogen fed to the sample for 16 h at 400 °C, (2) switched to 1% O_2 in nitrogen carrier gas to burn off saturated carbonate and formate surface species for an hour, (3) switched off O_2 and heated the sample cell to 600 °C for one hour in nitrogen-only to decompose surface PdO, (4) sample was cooled to 22 °C and stabilized over one hour. The IR spectra were collected with 64 scans at a resolution of 2 cm^{-1} in repeating loops every two minutes. A clean sample background was acquired first under flowing nitrogen then 1% CO was added to saturate the surface through two hours.

The mean Pd dispersion and particle size was determined with two methods. H_2 chemisorption was performed using a Micromeritics ASAP2020 instrument with a static volumetric adsorption/out-gas/re-adsorption method described by Chen et al. [19]. Prior to analysis, each sample was first degassed in N_2 at 500 °C, then cooled under vacuum to 1 microtorr prior to evaluation. Each sample was then reduced at 350 °C in pure H_2, (assumed to not sinter the Pd particles) then exposed to vacuum at 1 microtorr to remove Pd hydride prior to H_2 chemisorption measurements at 35 °C. A hydrogen adsorption stoichiometry value of 1 was assumed, for one adsorbed H atom per every one surface Pd atom. This technique is an improvement upon the classic H_2–O_2 titration method and avoids problems of H_2 spill-over and Pd hydride formation from interfering with the irreversible adsorbed H_2 calculation [36,37]. The differential results were used to report Pd dispersion and size to exclude physisorbed H_2 on the support. H_2 chemisorption was used for all samples since we found that CO chemisorption significantly overestimated the Pd dispersion on the CZO supports, probably due in part to CO adsorption on CZO forming stable carbonate species [38]. Post-process curve fitting of the XRD pattern Pd [1 1 1] peak was performed with the Rigaku PDXL software program. The software calculations used for estimating mean Pd crystalline length from XRD pattern line broadening was based on the Scherrer equation [39]. The shape factor used was 0.89 for spherical crystallites and the peak integral method was used to determine peak breadth. The instrument broadening was corrected with a LaB_6 calibration standard.

2.5. High temperature X-ray diffraction (HTXRD)

HTXRD was measured using a Bueler HDK furnace attachment mounted to a Scintag X1 diffractometer equipped with a low divergence (0.03°) beam of Cu-Kα radiation produced using an Osmic collimating optic. Data were collected using an Inel 120° position sensitive detector with a 250 mm radius. X-ray source settings were 45 kV and 40 mA. Scans were performed with an interval of 0.015°2θ. Samples were prepared by wet-milling 20 mg of powder in ethanol and pipetting it onto a 1 mm thick, 10 mm square silicon carbide single crystal slide and allowing to dry. The slide was then placed onto the primary heating strip that includes a Pt thermocouple welded to its underside for feedback temperature control. Calibration of the sample temperature was verified to be within +/−5 °C by comparing the observed melting transition in its HTXRD pattern to the known melting point of high purity aluminum. Gas flow into the furnace chamber was controlled with MKS mass-flow controllers at a total flow rate of 1 L/min. The internal volume of the furnace chamber was about 1.5 L. Oxidation experiments were conducted after an initial *in-situ* 1 h reduction in 250 sccm of 5% H_2 in balance N_2 at 300 °C. Prior to each experiment, the chamber was purged with pure N_2 for 5 min and the heating strip temperature was adjusted to the temperature of interest. HTXRD data were recorded with one scan during the purge to obtain the initial Pd [1 1 1] peak size and the feed gas was switched to dry air simultaneously with the beginning of an acquisition of repeated scans. The PdO phase fraction was calculated as one minus the quotient of the current integrated Pd peak area at time t divided by the initial Pd peak area at time zero. Temperatures used to collect HTXRD data were in the range of 200–350 °C.

2.6. Thermogravimetric analysis (TGA)

Thermogravimetric analysis (TGA) of PdO decomposition and Pd reoxidation was carried out in a TA Q500 instrument. About 77 mg of Pd/CZO sample was placed on the sample pan. The sample was preconditioned by holding at 400 °C in 10% O_2 environment and balance N_2 at 100 mL/min for 180–240 min for complete oxidation, then switching off O_2 and rebalancing with N_2, then holding in N_2 for 60–120 min at 100 mL/min while heating to 700 °C at a 5 °C/min ramp rate to decompose PdO. The oven temperature was then adjusted to one of two desired measurement temperatures, 350 °C or 700 °C, and held for 30 min before switching on the 10% O_2 to begin Pd oxidation. A Curie point temperature calibration using nickel (placed in the sample pan) confirmed the actual oven temperature is within +/− 2 °C of the set value.

2.7. TWC activity measurements

The ASAP2020 quartz j-tube that was fit onto a flow reactor measured 10.5 mm ID and was loaded with a catalyst sample mass of 0.30 g between 6 mm redistributing layers of quartz wool. The bed height for each Pd/CZO sample was 4 mm. Matheson dynablenders and flow controllers managed the gas flow through the system. A pyrex glass water bubbler was used to supply a stable stream of water vapor by saturation of the room temperature bulk gas stream. A solenoid set could be triggered to bypass the bulk gas around the water bubbler. The parts downstream of the water bubbler were stainless steel and wrapped in heat tape maintained at 150 °C to prevent condensation. The CO gas stream was scrubbed of iron carbonyls. Two K-type 1/32-inch diameter thermocouples were placed 16 mm before and 13 mm after the sample bed. A Hiden HPR20 quadrupole electron ionization mass spectrometer, pressure sensor and Horiba lambda sensor were used to sample the gas downstream of the j-tube. The HPR20 SEM detector measured five mass values in torr with a 2 Hz sampling rate at an inlet sampling pressure of 1E-5 torr. Two corrections were required to normalize the signals from other species into individual concentrations. First, the double excitation argon mass 20 value was scanned, which is 11% of the total argon level, rather than the typical mass 40 to get the measured argon value below the SEM detector limit of 1E-6 torr. Second, there was a CO and CO_2 mass overlap of 11.4%, so that amount of the CO_2 value was subtracted from the CO value during data processing.

Oxygen storage capacity (OSC) measurements were carried out by alternating one minute lean or rich exposures, each separated by a one minute purge. The purge pulse was just the constant bulk carrier gas of CO_2 and argon at 975 mL/min while microvalves added a square step pulse of CO or O_2 into the carrier gas at 25 mL/min. The bulk flow with lean pulse was 1% O_2, 2% CO_2 and balance Ar. The bulk flow with rich pulse was 2% CO, 2% CO_2 and balance Ar. The gas mixture was initially established at equilibrium over the catalyst sample at 50 °C. At least five CO pulses were measured at a

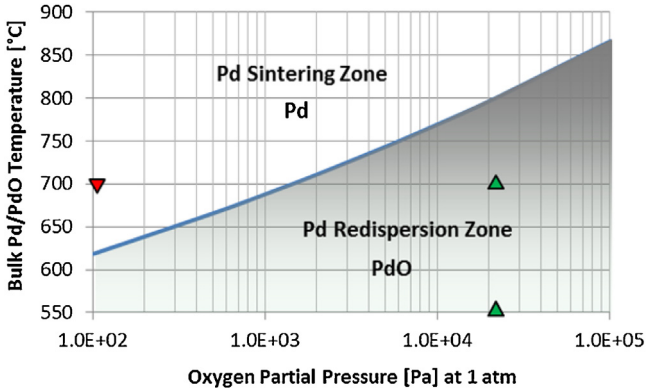

Fig. 1. Bulk palladium oxide thermal stability using a published equation from Ref. [26]: $\log(pO_2/1\,Pa) = 15.8–12300\,K/T$. The red triangle represents the lean aging condition of 0.1% O_2 that is 80 °C above the oxide decomposition temperature. The green triangles represent the lean treatment condition of 21% O_2 that are well below the oxide decomposition temperature. (For interpretation of the references to colour in this figure legend, the reader is referred to the web version of this article.)

fixed oven temperature before increasing the heating set point to the next 50 °C increment, to a maximum set point of 400 °C.

Water gas shift (WGS) measurements were carried out with a constant feed of bulk carrier gas made up of 2% CO, 2% CO_2, 2.5% H_2O and argon at a total flow of 1 L/min. The bulk stream of argon and CO_2 were fed through the water bubbler at 22 °C to saturate the bulk gas and later downstream the CO was injected at the microvalve. The gas mixture was initially established at equilibrium over the catalyst sample at room temperature before triggering the start of the heating ramp at 10 °C/min to 400 °C.

Multiple OSC and WGS tests were run to determine whether the results drifted with changes to the sample caused by exposure to the gas stream at 400 °C. At least three OSC and WGS measurements were run on all samples. The last run was usually selected for comparison to the other sample aging conditions.

3. Results

3.1. Catalyst aging and Pd redispersion zone

The catalyst aging and Pd redispersion conditions were compared to the results from Peuckert, which were used to develop an equation that predicts the bulk PdO decomposition temperature as a function of O_2 concentration [26]. The results from this equation are plotted in Fig. 1 for 1 atm total pressure. With just 0.1% O_2 in the lean-only and lean redox aging environments at 700 °C, the catalyst was above the bulk PdO decomposition temperature of about 620 °C. Lieske and Völter observed that Pd needed to be oxidized before redispersion would occur [23]. Incorporating the observations of Liekse and Völter, the area below the PdO decomposition line is shaded on Fig. 1 and labeled as the "Pd Redispersion Zone". Entry into the lower Pd redispersion zone was tested with lean treatments at 550 °C or 700 °C with dry gas containing 21% O_2/He or zero air, an environment where the supported catalyst was well below the bulk PdO decomposition temperature of about 800 °C. Farrauto et al. demonstrated that there was a hysteresis between the PdO formation and decomposition temperature in air that varied with support. For example, PdO on ceria decomposed during heating at 775 °C and Pd reoxidized during cooling at 730 °C [25]. At lower oxygen concentrations near 0.5% O_2, the support effects diminish and a supported PdO decomposition temperature is closer to the bulk PdO value in Fig. 1 as demonstrated by Colussi et al. on both Pd/Al_2O_3 and $Pd/CeO_2/Al_2O_3$ catalysts [40]. Therefore, once the PdO had decomposed into metallic Pd around 620 °C during heating under the redox or lean aging conditions at 700 °C, reoxidation of Pd would not occur until the temperature had dropped below the hysteresis temperature. Consequently, the supported Pd would likely be in the metallic state for all three aging environments.

3.2. Surface area and pore volume characterization

The BET surface area and BJH adsorption pore volume for each sample are listed in Table 1 below, both fresh and after exposure to various aging environments. The fresh Pd/CZO sample had a surface area of 91 m^2/g and a pore volume of 0.160 cm^3/g. The catalyst samples showed a loss in residual surface area after each aging duration interval, but in each case the lean-only aging environment was the least severe condition and the redox aging environment was the most severe aging condition after 2 h. The 2 h lean treatment caused some surface area loss when applied after 20 min of aging, while the 2 h and 16 h aged samples were more stable. All three 20 min aged samples showed an increased pore volume over fresh, perhaps from the aging temperature exceeding the calcination temperature, but the aging conditions soon sintered the pores as evidenced by the 2 h and 16 h data. The redox aging showed the most pore volume loss after 2 and 16 h. CZO is a reducible support under these conditions and the repeated redox cycling was more degrading to CZO than the other environments at 2 h and beyond.

3.3. XRD pattern phase identification

The XRD patterns of the fresh, aged and post lean treated samples of Pd/CZO are shown in Fig. 2 and are consistent with the expected peaks for a CZO support. The fresh sample Pd [1 1 1] peak was indistinguishable in the XRD pattern apart from the background. Fig. 2a shows the XRD pattern after 20 min of aging. A slight appearance of a peak at 40°2θ emerged for the redox sample with a peak maximum of 40% above the average background measured at 42°2θ. The 700 °C lean treatment applied to the redox aged sample caused the Pd [1 1 1] peak to vanish. A Pd [1 1 1] peak fit of the redox aged sample resulted in a bulk diameter of 20 nm, which was perhaps representing just the largest crystals. Pd particles less than 6 nm are often not distinguishable apart from the background XRD pattern. Therefore a significant number of the Pd particles on the 20 min redox aged sample were likely below the detectable threshold. Fig. 2b and c shows the XRD pattern after 2 h and 16 h of aging, respectively. A significant Pd [1 1 1] peak was observed at 40°2θ only for the redox and rich-only aged Pd/CZO samples. The 700 °C lean treatment decreased the area of the redox aged Pd [1 1 1] peak and shifted it slightly to a lower scattering angle of 39°2θ, indicating an expanded lattice that are similar to the shift observed with Fig. 2d β-$PdH_{0.64}$ (reference card 04-002-0377).

3.4. Average Pd size comparison

The apparent Pd dispersion and Pd particle size for each sample are listed in Table 1. The Pd metal dispersion (D) was estimated as a function of the Pd particle size (d_P) using Eq. (1) below, which is described further by Baylet et al. assuming spherical shapes [41].

$$D[\%] = \frac{\left(6 \times 10^5\right) \times (M_{Pd})}{(\rho_{Pd} \times S_{Pd} \times d_P\,[nm])} \quad (1)$$

With M_{Pd} as the Pd atomic weight of 106.4 g/mol, ρ_{Pd} as the Pd density of 12 g/cm^3, S_{Pd} as the molar surface area of Pd metal of 47,780 m^2/mol assuming an equidistribution of the low index faces.

The lean-only aging environment resulted in modest decreases in Pd dispersion with aging duration as measured by H_2 chemisorption. The redox and rich-only aging environments at 2 h and 16 h

Table 1
Support surface area and Pd size characterization of Pd/CZO samples.

Environment	Duration	N_2 Physisorption		H_2 Chemisorption	
		Surface area [m^2/g]	Pore volume [cm^3/g]	Pd dispersion[%]	Pd particle size [nm]
Fresh	–	91	0.160	22%	5.1
Lean-only 700 °C	20 min	66	0.162	19%	5.8
	2 h	59	0.160	16%	6.7
	16 h	49	0.159	13%	8.6
Rich-only 700 °C	20 min	59	0.166	u/d[a]	u/d[a]
	+550 °C/2 h air	53	0.152	3.6%[a]	30[a]
	2 h	52	0.159	u/d[a]	u/d[a]
	+550 °C/2 h air	48	0.154	2.9%[a]	38[a]
	16 h	46	0.154	u/d[a]	u/d[a]
	+550 °C/2 h air	44	0.154	2.0%[a]	55[a]
Redox (10 min lean/10 min rich) 700 °C	20 min	63	0.163	7.9%[a]	14[a]
	+550 °C/2 h air	60	0.156	12%	9.1
	+700 °C/2 h air	55	0.156	20%	5.4
	2 h	51	0.156	u/d[a]	u/d[a]
	+550 °C/2 h air	47	0.151	2.1%[a]	52[a]
	+700 °C/2 h air	52	0.158	13%	8.8
	16 h	41	0.150	u/d[a]	u/d[a]
	+550 °C/2 h air	40	0.152	1.3%[a]	84[a]
	+700 °C/2 h air	41	0.149	8.7%	13

[a] Pd particles suspected to be covered or partially encapsulated.

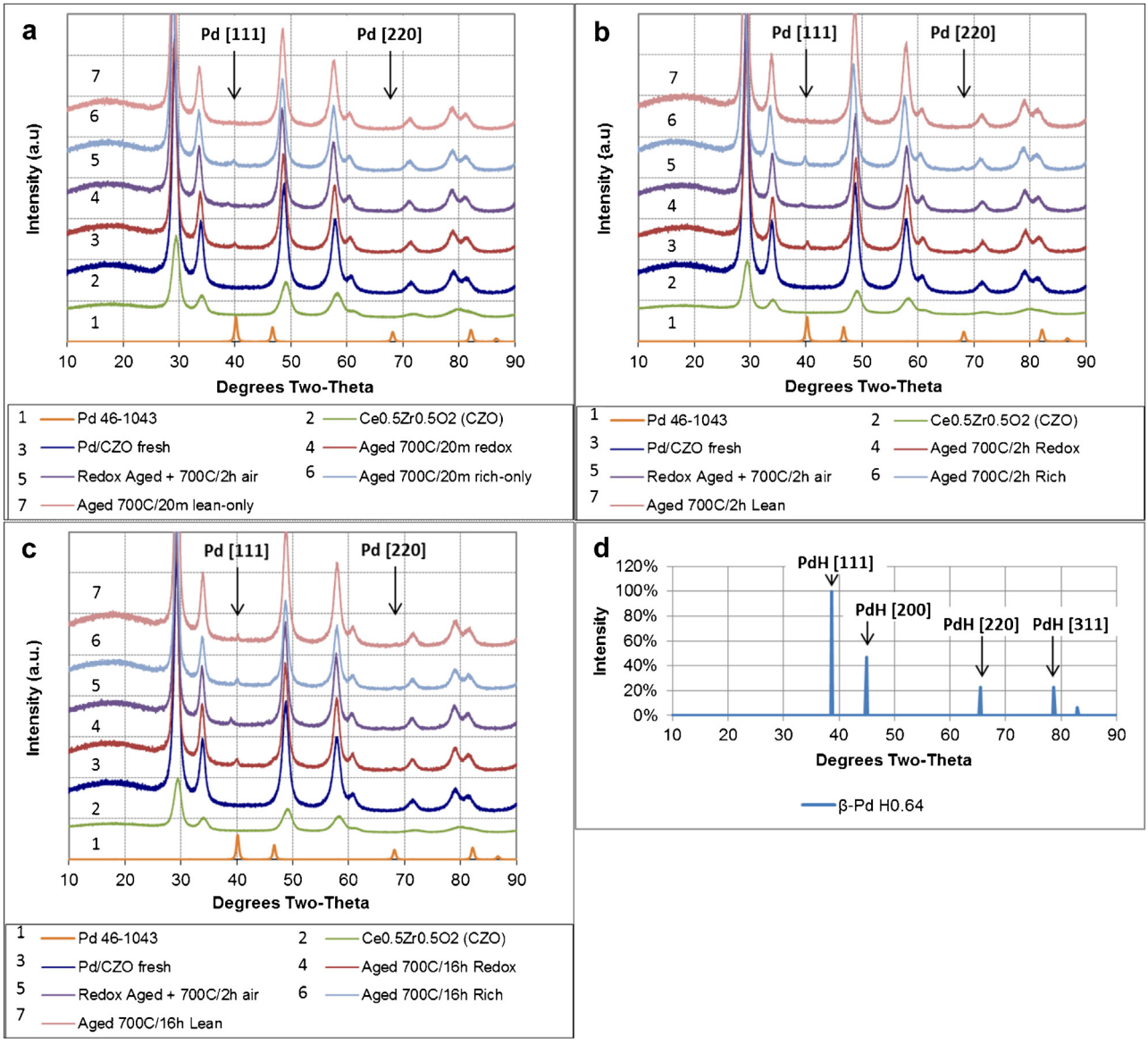

Fig. 2. XRD pattern results. Plots for: (a) 20 min aging, (b) 2 h aging, (c) 16 h aging, (d) reference β -PdH0.64.

Table 2
Comparison of Pd size characterization methods on Pd/CZO samples.

Environment	Duration	H_2 Chemisorption		XRD Pd [1 1 1] peak fit	
		Pd dispersion [%]	Pd particle size [nm]	Pd dispersion[%]	Pd particle size [nm]
Redox	2 h	u/d[a]	u/d[a]	6.5%	17
(10 min	+550 °C/2 h air	2.1%[a]	52[a]	5.3%	21
lean/10 min	+700 °C/2 h air	13%	8.8	10%	11
rich)	16 h	u/d[a]	u/d[a]	5.4%	20
700 °C	+550 °C/2 h air	1.3%[a]	84[a]	5.4%	20
	+700 °C/2 h air	8.7%	13	6.3%	18

[a] Pd particles suspected to be covered or partially encapsulated.

each had undetectable (u/d) Pd surface area as measured by H_2 chemisorption. H_2 chemisorption provides a quantitative measurement of the exposed metal surface. Strong metal support interaction (SMSI) with Pd under reducing conditions are known to confound the results of this technique, as any reducible oxide support material can decorate or otherwise chemically inhibit H_2 access to the metal surface [42,43]. The undetectable Pd surface area results after exposure to the rich-only conditions at 700 °C is consistent with SMSI effects, although perhaps surprising after just 20 min. At 20 min of aging. The 550 °C/2 h lean treatment provided a modest increase in Pd dispersion, while the 700 °C/2 h lean treatment restored the Pd dispersion completely to the level of the lean-only aging. These lean treatment Pd redispersion benefits diminished as the sample was allowed to accumulate a longer aging duration prior to the lean treatment application.

The changes in Pd size determined by H_2 chemisorption was checked against the trends observed in XRD pattern Pd [1 1 1] peak fit estimates as shown in Table 2. The XRD Pd size estimate is a volumetric average technique and the result should be larger than the estimate from chemisorption, which is a surface average technique, while both techniques are weighted towards larger particles. The Pd particles in Table 2 were 21 nm or less and within the size range in the literature of 2–33 nm where crystallite length is synonymous with particle size, as those works used electron microscopy and chemisorption for confirmation [44–47]. Note that crystallite length can be smaller than particle size if large particles are made of agglomerated crystals of if any poorly crystalline regions exist in the particle. The fresh and 20 min aged samples were excluded from Table 2 as very small metal crystallites have excessively broad peaks that would not be completely detectable apart from the support diffraction pattern, since the width of the X-ray diffraction peak is inversely related to the crystallite length. The 2 h and 16 h rich-only and redox aged samples both showed Pd particles that were 17 nm and 20 nm, respectively by XRD, which would result in 5–6% dispersion if the Pd particles were not covered by support material through SMSI effects. No Pd size decrease was observed by XRD following the 550 °C/2 h lean treatment. However, the 700 °C/2 h lean treatment did show nearly a 33% reduction in Pd size on the 2 h redox aged sample, yet a 10% reduction in Pd size on the 16 h redox aged sample. After the 700 °C/2 h lean treatment, reasonable agreement in Pd size was shown for the two characterization techniques, since the SMSI effect was removed by oxidation and the sintered Pd particles were large enough to be detected apart from the background pattern. The XRD Pd size results confirm the diminishing benefit of the 700 °C lean treatment the longer the sample is allowed to age.

3.5. XPS surface characterization

The XPS spectra of the fresh and redox aged Pd/CZO samples are shown in Fig. 3. The Pd 3d peaks were fit under the raw data between the shoulders of the Zr 3p peaks as is typically performed for analysis of Pd on CZO support [48–51]. The fresh Pd/CZO sample had two Pd 3d $_{5/2}$ peaks, at 334.7 eV for Pd metal and at 337.1 eV for Pd^{+2}. These results are consistent with those reported for Pd foil at 334.9 eV and PdO at 336.8 eV [52]. Pd peak shifting, due to redox aging or after a lean treatment, was not significant. However, redox aging suppressed the intensity of the Pd^0 peaks and eliminated the Pd^{+2} peaks. The 700 °C/2 h lean treatments restored the Pd^{+2} peaks, in spite of the mild reduction pre-treatment. Four more 700 °C/30 min lean treatments were needed with the 16 h aged sample to achieve almost the same benefit observed with one lean treatment on the 2 h aged sample.

The XPS spectra of the Ce 3d peaks are shown in Fig. 4. Neither the Ce 3d $_{5/2}$ peak at 882.0 eV or the Ce 3d $_{3/2}$ peak at 900.4 eV showed a shift due to redox aging or lean treatments. The other Ce 3d peaks shown are satellite peaks that arise from interactions with the Ce 4f valence electrons after the 3d core electron is emitted. Each core level (3d $_{5/2}$ and 3d $_{3/2}$) has 3 satellite peaks associated with it: the 3d $_{5/2}$ satellite peaks at v' = 884.0 eV, v'' = 889.1 eV and v''' = 897.8 eV; and the 3d $_{3/2}$ satellite peaks at u' = 903.2 eV, u'' = 908.1 eV and u'''' = 916.3 eV. The u''' intensity varies linearly with the amount of Ce^{+4} and is fairly well separated from the rest of the peaks, enabling better estimation of the background. We can compare the signal from u''' to the intensity of the total envelope to get the percentage of Ce^{+4} on the surface. This technique is further described elsewhere [52].

The atomic concentrations from the top surface layers are shown in Table 3 based on the peak intensities shown in Figs. 3 and 4. Adventitious carbon formed from exposure to room temperature air during the sample transfer and pellet pressing. While all catalyst samples were initially reduced prior to XPS evaluation, about half of the fresh Pd was still Pd^{+2}, perhaps due to an abundance of interface sites with finely dispersed Pd and oxygen from CeO_2. After 2 h of redox aging, the surface concentration of Pd^{+2} species vanished and the total Pd signal was decreased by 70% relative to fresh. The 700 °C lean treatment applied to the 2 h aged sample restored Pd over the surface, reestablished the Pd^{+2} bonds with Ce up to the fresh level and lowered the surface concentration of Ce^{+3}. After 16 h of redox aging, the surface concentration of total Pd was decreased by 70% coincident with a surface concentration increase in Ce by 15% and Zr by 10%, relative to fresh, without a significant increase in oxygen. This effect is consistent with Pd surface coverage by Ce [53]. The 700 °C lean treatment applied to the 16 h aged sample restored Pd over the surface, reestablished the Pd^{+2} bonds with Ce to near half of the fresh level and lowered the surface concentration of Ce^{+3}. Another four 700 °C lean treatments in 30 min durations increased the amount of Pd^{+2}, but again not to the level of the fresh catalyst. This improvement of exposed Pd surface from redox aged to 700 °C/2 h air regeneration agrees with the H_2 chemisorption measurements in Table 1. XRD does not detect surface coverage by support, but does confirm that the Pd particle size decreased following the lean treatment from 17 nm to 11 nm for the 2 h redox aged sample and from 20 nm to 18 nm for the 16 h redox aged sample as shown in Table 3. These Pd particle sizes are all within the detection depth of the XPS instrument so the dramatic loss in Pd surface concentration from fresh to redox aged in Table 3 was most likely due to CZO support coverage and not Pd sintering.

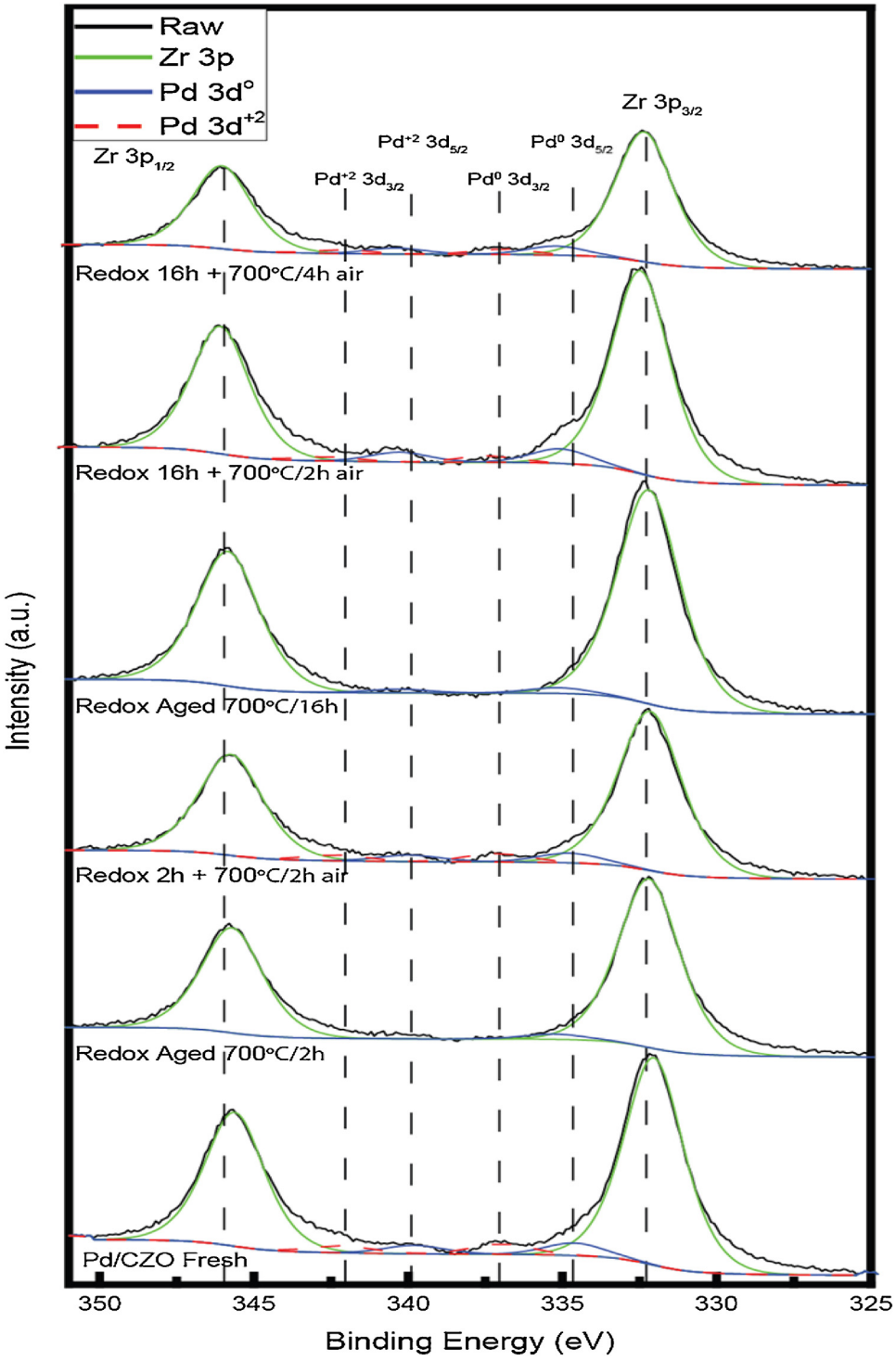

Fig. 3. XPS surface analysis of Pd 3d. Solid blue lines are representative fits for Pd metal, dashed red lines are representative fits for Pd^{+2}. Spectra are offset for clarity. (For interpretation of the references to colour in this figure legend, the reader is referred to the web version of this article.)

Table 3
Atomic surface concentrations of fresh and aged Pd/CZO samples by XPS.

Duration	Sample	C	O	Ce^{+3}	Ce^{+4}	Zr	Pd^0	Pd^{+2}
0 min	Fresh	20.9	59.9	2.0	4.0	12.6	0.29	0.28
2 h	Redox 700 °C	24.9	58.6	1.4	4.0	10.8	0.16	–
	+700 °C/2 h air	25.2	58.8	1.2	4.6	9.4	0.40	0.29
16 h	Redox 700 °C	22.8	56.2	1.9	5.0	13.9	0.16	–
	+700 °C/2 h air	24.1	57.8	1.3	4.3	11.9	0.35	0.16
	+700 °C/4 h air	27.9	54.1	1.3	4.2	11.9	0.35	0.21

3.6. Infrared measurements

The wave numbers characteristic to CO adsorption onto ceria, single Pd crystals and supported Pd particles are well studied [54–57] and summarized in Table 4. However, the IR band wave numbers are known to change with temperature, pressure and CO coverage [58,59]. Therefore the corresponding species given in Table 4 are approximate.

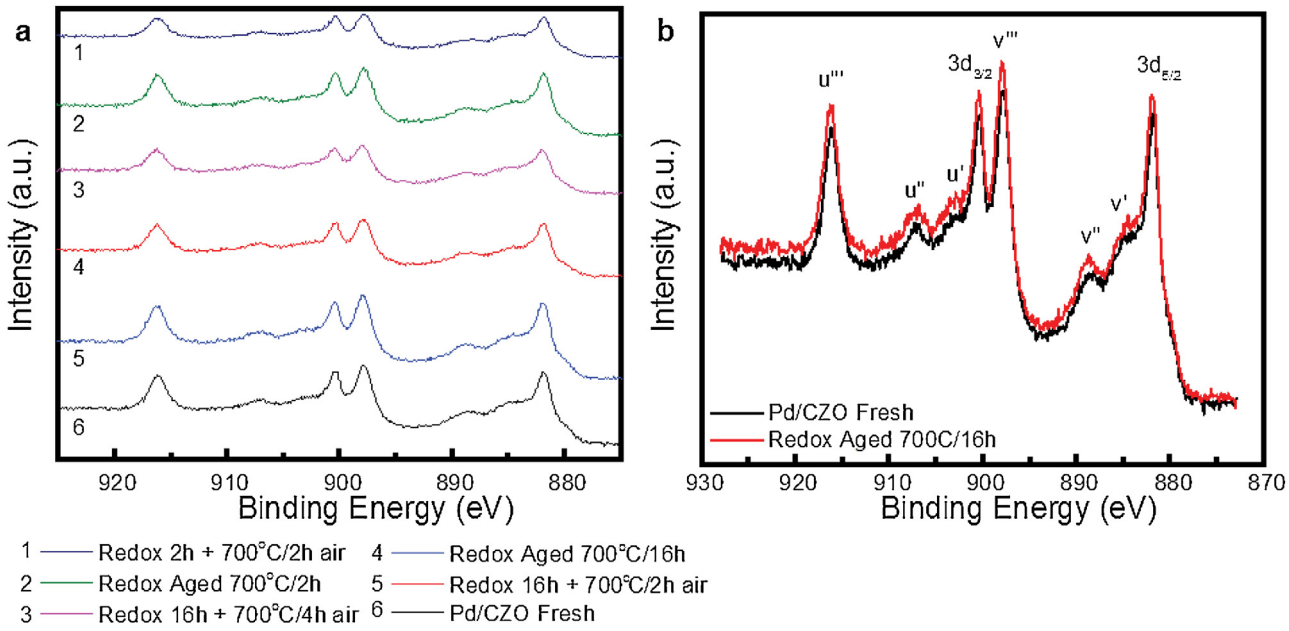

Fig. 4. XPS surface analysis of Ce 3d. Spectra are offset for clarity. Plots: (a) Fresh and redox aged samples and (b) identified satellite peaks.

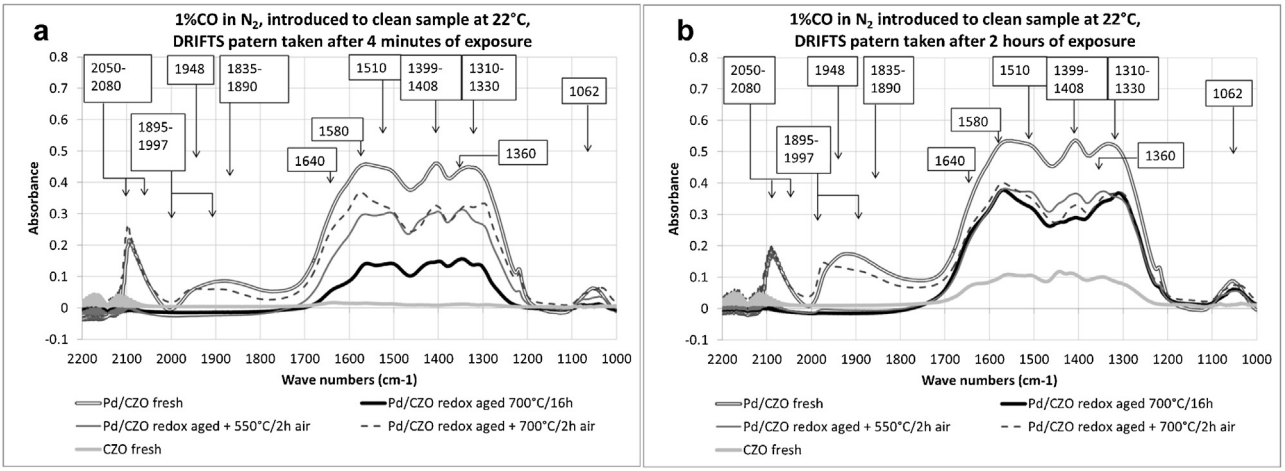

Fig. 5. IR spectra during CO exposure to clean samples at 22 °C. Plots: (a) after 4 min, (b) after 2 h.

Table 4
IR bands on CZO and Pd.

Species	Wave number [cm^{-1}]	Reference
Carbonates bidentate	1028, 1286, 1562	[54]
Carbonate unidentate	1062, 1454	[54]
CO–Ce^{+4} linear	1310–1330	[54]
Formates	1360, 1580	[54]
Hydrogen carbonate	1399–1408	[55]
Inorganic carboxylate	1510, 1560	[54]
Aromatic C=C bending	1500–1700	[56]
C=O stretch	1650	[56]
CO-Pd [1 1 1] bridge x3	1835–1890	[57]
CO–Pd [1 1 1] bridge x2	1948	[57]
CO–Pd [1 0 0] bridge x2	1895–1997	[57]
CO–Pd [1 1 1] linear	2050–2080	[57]

Fig. 5 shows the IR spectra of uncatalyzed CZO and Pd/CZO samples during CO adsorption at 22 °C. Spectra of the adsorbed species are the difference between the absorbance of the CO saturated sample and the clean sample background. As spectra for all samples were collected during flowing CO, gas phase CO appears as two similar bands starting at 2050 cm^{-1} through 2200 cm^{-1} with high frequency and low amplitude. The peaks for CO adsorbed on Pd linear and bridge sites from 1800 to 2000 cm^{-1} are shown for just the fresh and redox aged with 700 °C/2 h air treatment samples. The similarly sized CO-Pd linear adsorption IR peak at 2050–2080 cm^{-1} for these two samples suggests a comparable number of these sites, but the CO-Pd bridge sites appear more abundant for the fresh sample likely due to higher Pd dispersion results from Table 1. CO adsorption onto Pd is not observed for the Pd/CZO redox aged or Pd/CZO redox aged with 550 °C/2 h air treatment samples through two hours, which aligns with the undetectable chemisorption results from Table 1 for these samples, and provides evidence for coverage of Pd by SMSI with CeO_2 due to exposure to a high temperature reducing environment, in agreement with Badri et al. [30], since ZrO_2 is not reducible under these conditions.

The growth rate of carbonates and formates from 1000 to 1700 cm^{-1} in Fig. 5 showed the following trend: fresh Pd/CZO > Pd/CZO redox aged with 700 °C/2 h air > Pd/CZO redox aged with 550 °C/2 h air > Pd/CZO redox aged » CZO. This large difference between uncatalyzed CZO and the Pd/CZO samples implies

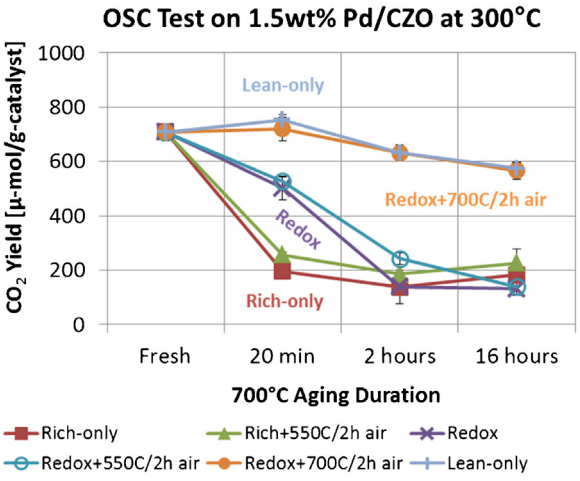

Fig. 6. OSC test on Pd/CZO samples CO_2 yield as a function of age.

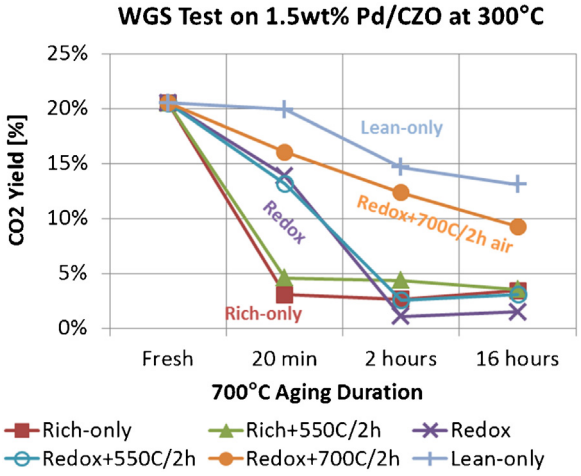

Fig. 7. WGS test on Pd/CZO samples CO_2 yield as a function of age.

that Pd enhances the formation of carbonates and formates at the Pd-CZO interface sites. For the Pd samples, the growth rate appears to be directly related to Pd dispersion results in Table 1. The difference in growth rate provides supporting evidence for the H_2 chemisorption results reported in Table 1.

3.7. Catalytic activity

CO_2 production can be measured directly by the mass spectrometer in units of partial pressure (i.e, torr) and can be combined with the other measured gas species to determine the total pressure and thus enable a relative concentration calculation for each gas species. Micromoles of CO_2 per gram of catalyst can be calculated for the OSC experiment using Eq. (2) below where the average CO_2 20 s before and after the CO pulse is used as the background:

$$\text{OSC } CO_2 \left[\frac{\mu\text{moles}}{\text{g}}\right] = \frac{(\text{current } CO_2\,[\%] - \text{background } CO_2\ [\%]) \times (\text{CO pulselength } [\text{m}]) \times \left(\text{gasflow rate } \left[\text{L/m}\right]\right)}{\left(22.414\left[\text{L/mole}\right]\right) \times (\text{mass } [\text{g}])} \quad (2)$$

Conversion of CO to CO_2 during the WGS experiment can be calculated using equation 3 below where the average CO_2 at room temperature is used as a background:

$$\text{WGS conversion of CO to } CO_2\,[\%] = \frac{100 \times (\text{current } CO_2 - \text{background } CO_2)}{(\text{CO at room temperature})} \quad (3)$$

The generation of CO_2 over the Pd/CZO samples at 300 °C is shown in Fig. 6 for the OSC test and in Fig. 7 for the WGS test. In each case the lean-only aging environment was the least deteriorated. The rich-only aging environment was the harshest environment after 20 min, but after 2 h the redox environment was the worst. The 550 °C/2 h lean treatment showed a modest improvement for the rich-only and redox aged samples, but the 700 °C/2 h lean treatment achieved restoration up to the lean-only aged sample. The OSC test of the most active catalysts at 350 °C and 400 °C showed complete consumption of CO so that the CO_2 conversion results were limited relative to the poorer catalysts. In all cases, the poorest performing catalysts were also the ones that had below 4% Pd dispersion measured by H_2 chemisorption as shown in Table 1.

3.8. PdO formation observed by HTXRD

PdO formation observed in air by XRD measurement of Pd [1 1 1] peak disappearance required samples that had well-defined Pd [1 1 1] peaks as shown in Fig. 2. This study therefore excluded the 20 min aged samples and the lean-only aged samples at all durations. In addition, we sought to avoid confounding of the Pd oxidation rate by SMSI effects such as partial encapsulation or decoration of Pd with Ce^{+3}. Therefore the 2 h and 16 h redox aged plus 700 °C/2 h lean treated samples were selected. The difference in bulk Pd size between these samples as shown in Table 2 was assumed significant enough to provide discrimination of PdO reoxidation rates.

Long sampling times were required for acceptable signal to noise diffraction patterns due to the large width of the beam (~1 mm) and the limited positional resolution of the detector (0.3 mm), causing relatively low instrumental resolution (~0.36°) compared to conventional focusing diffractometers. Fig. 8 shows the results of scans acquired at various durations to observe the Pd [1 1 1] peak from the Pd/CZO redox aged sample. The signal to noise ratio is defined as the signal average divided by the standard deviation of the background, and a value of at least 5 is considered sufficient for distinguishing features from the background. The Pd [1 1 1] peak was well resolved apart from the background and not affected by the CZO support peaks as shown in Figs. 2 and 8. Scans were spaced at 0.015°2θ intervals, providing 64 data points across each 1°2θ interval. The signal value was the average peak height at 38.8–39.8°2θ minus the average height of the background at 37–38°2θ and 41–42°2θ. The initial signal to noise ratio for the data in Fig. 8 was 6 for the four minute scan, while it was 4 for the two minute scan. Therefore

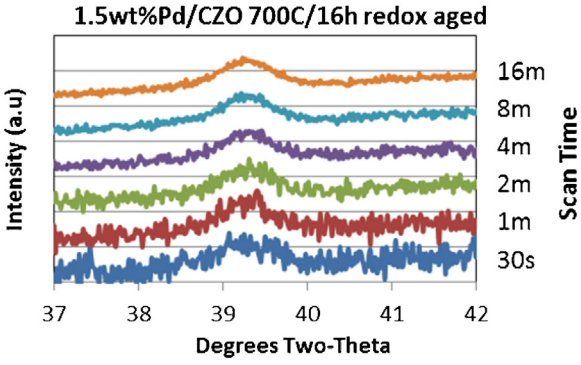

Fig. 8. HTXRD data acquisition scans with Pd [1 1 1] on CZO.

Table 5
Avrami model rate constant and exponent for measured PdO formation.

Temperature	Redox aged 700 °C/2 h + 700 °C/2 h air		Redox aged 700 °C/16 h + 700 °C/2 h air	
T (°C)	k (1/s)	n	k (1/s)	n
200	2.06×10^{-5}	0.37	1.14×10^{-5}	0.44
250	5.75×10^{-5}	0.43	2.79×10^{-5}	0.42
300	1.64×10^{-4}	0.36	7.72×10^{-5}	0.29
350	9.45×10^{-4}	0.29	3.24×10^{-4}	0.28

the four minute scan was considered an effective balance between fast data acquisition and low noise.

The long measurement times needed to monitor the Pd particle growth limited the accessible temperature range of the measurement. At sufficiently high temperatures, the growth of Pd particles becomes too fast for the HTXRD measurement acquisition time needed and an alternative method is needed to estimate the growth rate. To enable this approach, an accurate model of the time dependence of the growth is needed. The calculations used for the PdO phase fraction appearance during the HTXRD experiment are based on the Avrami–Erofe'ev model equation for the kinetics of phase transformations [60,61]. The linearized Avrami–Erofe'ev model equation relates the growth of an emerging phase fraction α at time t, rate constant k, and growth exponent n as shown by Eq. (4) below.

$$\alpha = 1 - \exp(-kt)^n \tag{4}$$

By plotting the phase fraction against time on a log–log scaling, k and n can be easily extracted assuming a linearized version as shown by Eq. (5) below.

$$\ln\left(\ln\left[\frac{1}{(1-\alpha)}\right]\right) = n \times \ln(k) + n \times \ln(t) \tag{5}$$

The values of k were then plotted against inverse absolute temperature to determine the Arrhenius relationship and extract the activation energy E_a and frequency constant A by fitting the rate constants at the temperatures of each measurement by Eq. (6) below:

$$k = A \times \exp\left(\frac{-E_a}{RT}\right) \tag{6}$$

An XRD pattern with the initially reduced Pd [1 1 1] peak at a low temperature of interest was acquired under nitrogen and the area under the peak was integrated for the 100% Pd baseline at time zero (t_0). Once complete, air was introduced and acquisition began immediately of XRD patterns for the measurement of the Pd [1 1 1] peak at each time interval (t). At each scan time interval (t), Pd [1 1 1] (t) was equal to the peak intensity integrated from 38.8–39.8° 2θ minus the background intensity integrated from 37–38° 2θ and 41–42° 2θ. The PdO fraction at time t was determined by Eq. (7) below:

$$\mathrm{PdO}(t) = 1 - \left(\frac{\mathrm{Pd}[111](t)}{\mathrm{Pd}[111](t_0)}\right) \tag{7}$$

The PdO formation rate increased as a function of time and temperature as shown in Fig. 9, plots a and b. The measured data was fit using the linearized Avrami model, yielding similar slopes with discrete intercepts at each measured temperature. Table 5 lists the average growth constant, n, and oxidation rate, k, determined from the fits in Fig. 8 of the slope and intercept, respectively. The average value of the growth parameter n was 0.36 across the measured temperature range, corresponding to a $t^{0.36}$ relationship in the Avrami model, is similar to the $t^{1/3}$ growth relationship with fine Pd powder oxidation as studied by Matsui et al. [62]. Fig. 10 shows a linear trend of the reaction rates plotted as an Arrhenius relationship with each measured temperature. Fig. 10 lists the linear data fit equation, and activation energy, E_a, and constant, A, determined from the slope and intercept of the data fits. The rate parameter, k, for the 2 h redox aged/regenerated sample was about twice that of the 16 h redox aged/regenerated sample for each temperature. From Table 2, the Pd particle size of the 2 h aged/regenerated sample was 8.8 nm by chemisorption or 11 nm by XRD while the 16 h aged/regenerated sample was 13 nm by chemisorption or 18 nm by XRD. Therefore the smaller Pd size (and higher Pd dispersion as per Eq. (1)) led to faster oxidation. It is therefore important to keep Pd smaller than 8.8 nm to achieve rapid oxidation for possible redispersion during a brief vehicle fuel cut.

The above point can be further emphasized through a simplified extrapolation of the PdO formation rate at 700 °C by working the above process in reverse. An extrapolated rate k at 700 °C may be determined with Eq. (6), since E_a and A are known, then the PdO formation with time at 700 °C may be determined with Eq. (4) with the average n value of 0.36 and the extrapolated rate k. Given a 10 s fuel cut at 700 °C, such an extrapolation for each Pd/CZO sample would yield as follows: the 2 h aged/regenerated sample would have 55% PdO while the 16 h aged/regenerated sample would have 37% PdO, assuming no initial PdO, uncovered Pd surfaces and a dry air environment. So it is important to maintain Pd particles smaller than 8.8 nm as neither sample was predicted to be completely oxidized within 10 s. However, any high temperature extrapolation may not hold up to scrutiny given expected Pd sintering at 700 °C (demonstrated by our aging results) or support coverage of Pd by SMSI in redox conditions in as little as 20 min. Sintering rates and SMSI of Pd are negligible under the measurement conditions at 350 °C in nitrogen, or during the air pulse, and are not reflected in the measured parameters.

3.9. PdO formation observed by TGA

Fig. 11 shows the result of TGA measurements for PdO decomposition in N_2, and confirmation of the HTXRD measurements of PdO formation rate at 350 °C and the simplified extrapolation of the PdO formation rate at 700 °C. The sample used for TGA analysis was the same 16 h redox aged/regenerated sample from the HTXRD measurements. However, the initial condition of the sample had to be different for the two techniques. The TGA sample was oxidized to limit confounding weight gain by CZO oxygen uptake, while the HTXRD sample was reduced in order to view the Pd [1 1 1] peak. Fig. 11a shows the PdO decomposition plot in N_2 to 700 °C used to prepare the Pd metal for oxygen uptake. The derivative weight shows peak oxygen release near 600 °C. The maximum theoretical weight gain for the complete Pd oxidation of 77 mg of 1.5wt% Pd/CZO sample was determined to be 0.174 mg. The actual weight loss of 0.146 mg reveals a reduction of 84% compared to the theoretical value, so the weight loss could be from just the PdO and not the CeO_2 in the support. The sample oven temperature was then adjusted to either 350 °C or 700 °C. In both Fig. 11b and c, 10% O_2 was fed to the sample and a weight gain was observed. The calculated theoretical maximum weight gain of 0.174 mg was multiplied by the PdO formation fraction measured by HTXRD or extrapolated as a function of time by Eq. (4) above to obtain the weight gain by HTXRD in air. Weight gained was divided by the calculated theoretical maximum to obtain a fraction of PdO formation by TGA in 10% O_2. For Fig. 11b and c, the results with TGA in 10% O_2 was similar in trend, yet just below that observed with HTXRD in air. The difference in Pd oxidation for the two techniques may be due to the higher amount of oxygen in the HTXRD feed stream or the lower extent of Pd reduction prior to the oxidation pulse with the TGA sample. The good consistency of the TGA and HTXRD measurements allows for estimation of the oxidation rates to temperatures beyond the range accessible by the HTXRD method. From the extrapolation, we are

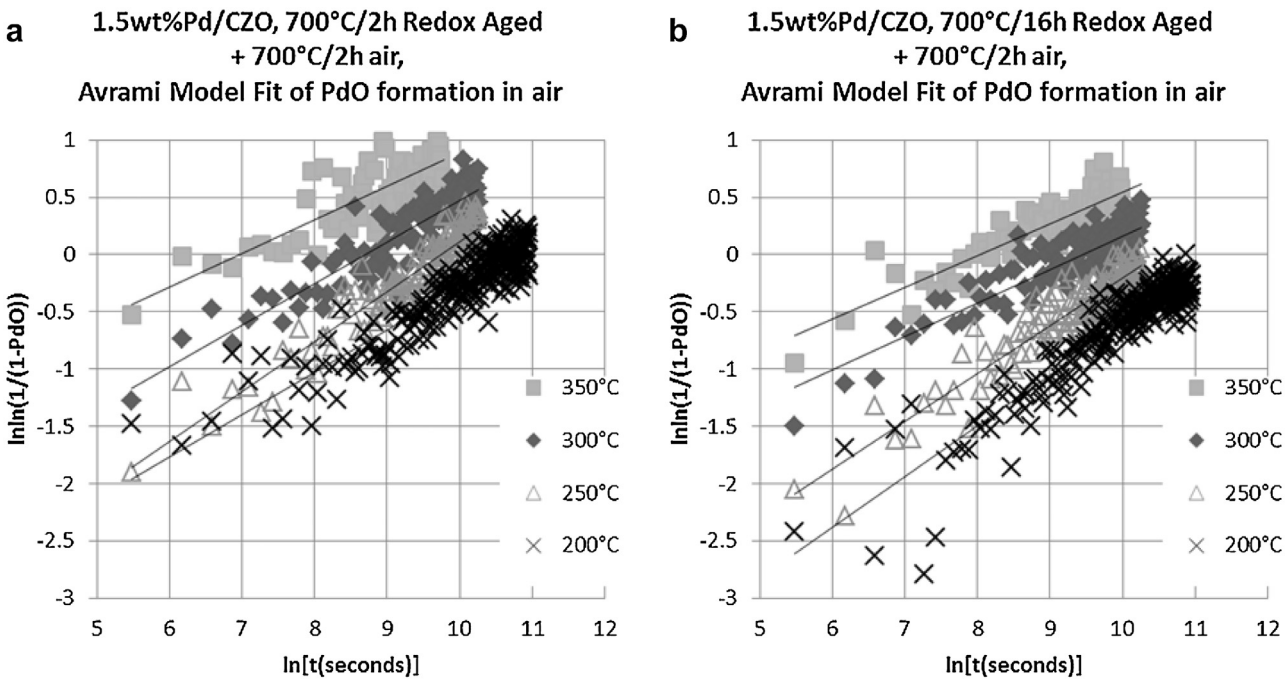

Fig. 9. Measured and fit PdO formation rates in air at low temperature. Plots of redox aged-regenerated samples: (a) 2 h fit data, (b) 16 h fit data.

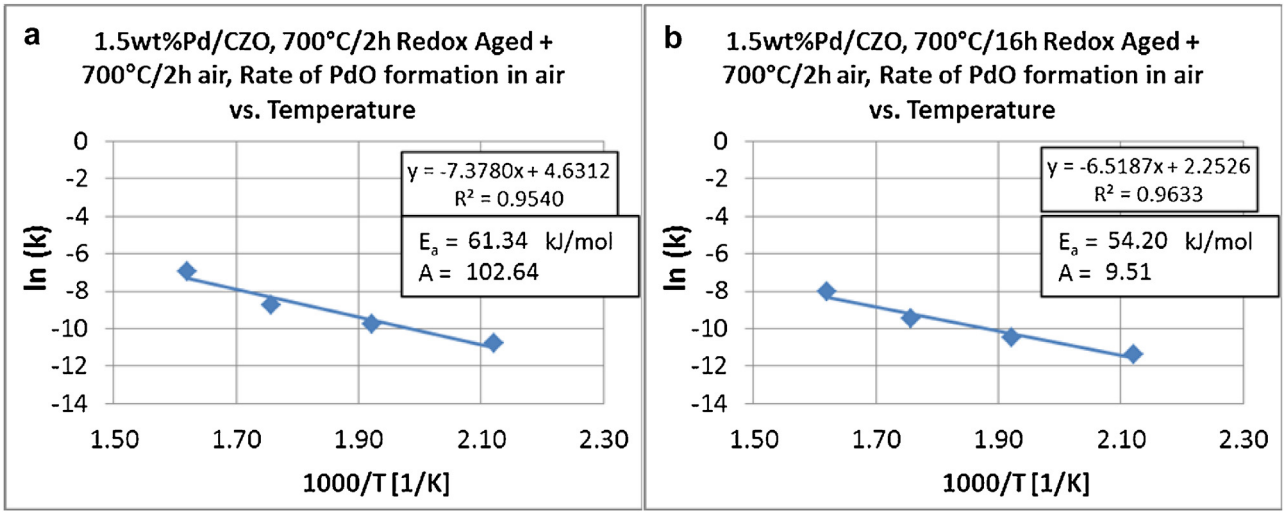

Fig. 10. Arrhenius model fit of PdO formation rates in air at low temperature. Plots of redox aged-regenerated samples: (a) 2 h fit data, (b) 16 h fit data.

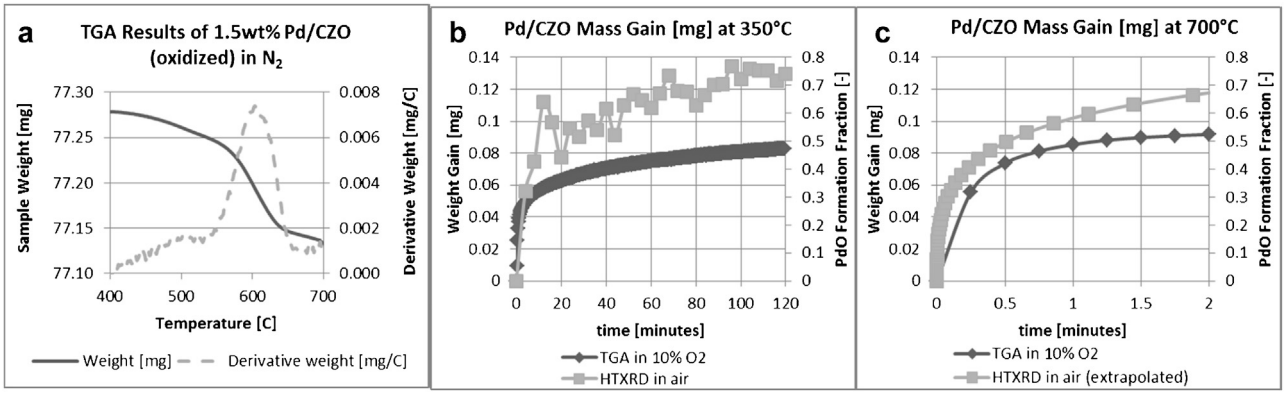

Fig. 11. TGA results on Pd/CZO redox aged 700 °C/16 h + 700 °C/2 h air. Plots: (a) PdO decomposition in N_2, (b) comparison to HTXRD results at 350 °C, (c) comparison to HTXRD results extrapolated to 700 °C.

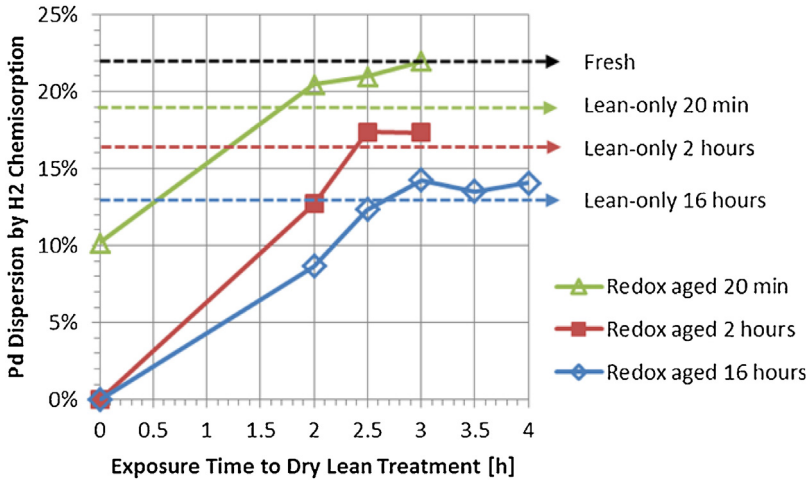

Fig. 12. Effect of additional dry lean treatments.

able to further estimate the effectiveness of the lean treatments to achieve redispersion and infer a recommendation for a practical engine control strategy.

3.10. Effect of additional brief lean treatments

Fig. 12 shows the result of additional dry lean treatments on the Pd dispersion for the redox aged samples. With one 2 h lean treatment, these redox aged-regenerated samples showed lower dispersion than the equivalent duration lean-only aged samples, except for the 20 min redox aged-regenerated sample, which was just above the level of the lean-only 20 min aged sample. The 20 min redox aged sample may not have had the Pd covered by CZO after redox aging, but no confirmation of Pd redispersion by XRD was possible to confirm the improvement shown by H_2 chemisorption in Table 1. Additional 30 min pulses of dry air at 700 °C were applied to achieve essentially complete oxidation of Pd on both samples with each pulse. The 20 min redox aged-regenerated sample showed slight increases in Pd dispersion with each 30 min dry air pulse up to the fresh level. The 2 h redox aged-regenerated sample showed a substantial increase in Pd dispersion with the first 30 min dry air pulse to just above the level of the lean-only 2 h aged sample, but the second 30 min dry air pulse showed no further improvement. The 16 h redox aged-regenerated sample also showed a substantial increase in Pd dispersion with the first 30 min dry air pulse, but the result was just below the level of the lean-only 16 h aged sample. A second 30 min dry air pulse showed further improvement to above the level of the lean-only 16 h aged sample, but the next two pulses did not bring further improvement. Multiple lean treatments were likely needed due to the CZO support covering the Pd surface after redox aging, where the first pulse decomposed the CZO that prevented some PdO wetting and spreading. It appears that the lean treatment has limitations with improving Pd dispersion to the equivalent duration lean-only aged sample and this upper limit may be linked to residual catalyst surface area.

4. Discussion

4.1. Aging environment

Model powder catalysts showed dynamic changes to Pd dispersion depending on oxygen concentration in the 700 °C aging environment. For the Pd/CZO samples, the rich-only and redox environments caused much more severe loss of Pd dispersion than the fixed lean-only exhaust gas compositions, producing samples with the lowest activity for the WGS and OSC tests. Exposure to dry air at 700 °C caused the Pd dispersion to increase as measured by both H_2 chemisorption and XRD techniques. Based on these observations, one approach to maintain Pd dispersion on a catalytic converter is to manage engine operation so that the exhaust gas composition falls along a trajectory that avoids the fuel-rich environment or includes periodic fuel shut-off events during high speed driving conditions to reoxidize Pd into PdO to redisperse the Pd.

4.2. Aging duration

Studies on Pd sintering have shown the rapid particle agglomeration and loss of Pd dispersion as a function of aging duration [3,8]. Recent studies of atomically dispersed Pd noted that subnanometer agglomerates of Pd atoms were easy to redisperse through a 700 °C calcination, while larger PdO particles were found to be very stable in air and did not sinter up to 800 °C [24,63]. Peterson et al. speculated that the stability of bulk PdO may not allow it to be so easily redispersed as smaller Pd particles [63]. This agrees with earlier observations linking Pd particle size to the onset of PdO formation, wetting, spreading and rupture [20,23]. Our focus here was to determine for how long operation at highway driving exhaust temperatures could be maintained while still allowing for effective regeneration of the activity lost due to Pd agglomeration. As the Pd/CZO catalyst is aged longer, the lean treatment becomes less effective and appeared to become limited to the dispersion achieved after lean-only aging as shown in Fig. 12. Still, the 2 h redox aged sample was able to achieve significant Pd redispersion comparable to that produced in the lean-only aged sample (13% vs. 16%). However, there is another important factor to consider: Pd redispersion first requires PdO formation and only Pd particles of a size just a few nanometers in diameter could achieve reoxidation and redisperse during the mere seconds of air that would be supplied by a typical fuel cut. Based on the measured Pd oxidation rate and the measurements of Pd size by chemisorption, the 8.8 nm Pd particles had twice the oxidation rate of the 13 nm Pd particles. In addition, the simplified extrapolation of PdO formation on the 8.8 nm Pd particles at 700 °C suggests that even 10 s in air is not enough to achieve over 60% oxidation of Pd. Therefore a fuel cut should be performed before the Pd particles reach 8.8 nm in diameter to enable the lean treatment to be more efficient, which suggests a fuel cut just after 20 min of 700 °C stoichiometric (i.e., redox) operation. Depending on the aging history of the catalyst, this fuel cut frequency can be adapted to continuously maintain proper catalyst performance through lean Pd redispersion.

Due to the limitations of XRD for discerning finely dispersed Pd particles apart from the background pattern, we were not able to measure the PdO formation rate on the 20 min redox aged-regenerated sample. Newton et al. acquired Pd oxidation data taken at the European Synchrotron Radiation Facility (ESRF) on Pd nanoparticles of 3 nm in diameter [28]. Further synchrotron work could be done to study Pd particles below an 8.8 nm diameter.

4.3. Support effects

The benefits of lean treatments on Pd were slightly confounded by the SMSI effect between Pd and CeO_2. In an electron microscopy study, Chen and Ruckenstein observed Pd on an alumina film with microscopy in a pure oxygen environment and observed that the smallest PdO crystallites (<15 nm) wet and spread over the surface at 350 °C while the larger PdO crystallites did not [20]. Then at 500 °C, all PdO crystallites eventually moved about the surface, rupturing and fracturing of the spreading Pd crystallites was observed as a mechanism to form smaller particles. In our work, the 550 °C regeneration on 16–20 nm Pd particles should have had an effect similar to that observed by Chen and Ruckenstein, but XRD did not confirm any significant bulk Pd crystal size decrease. Our XPS and DRIFTS results showed substantial coverage of the Pd by the CZO support that likely limited the mobility of Pd wetting and spreading over CZO. Other work has shown that ceria covering a Pd surface can be removed from just the Pd [1 1 1] surface when heated in air at 500 °C [30], and completely decomposed when heated in air at 700 °C [53]. These observations may explain the difference in Pd size reduction accomplished on the redox and rich-only aged Pd/CZO samples with the lean treatments at 550 °C versus 700 °C.

Pd was able to redisperse on the CZO support material as evidenced by the catalyst activity improvement and measured Pd size reduction of the 700 °C lean treated redox aged samples versus the as-is redox aged samples. These results are consistent with Hickey et al. using Pd supported on $Ce_{0.68}Zr_{0.32}O_2$ and aged on a redox cycle, showing a lower temperature for conversion of CO after a high temperature lean treatment although no chemisorption results were reported to demonstrate a lower Pd size [18]. Peterson et al. showed supported Pd clusters treated in air at 700 °C or with 1% O_2 achieved atomically dispersed Pd^{+2} species that were more stable on La_2O_3–Al_2O_3 than on undoped alumina [63]. The observations of Peterson et al. also are consistent with our XPS results where Pd^{+2} was observed on the lean treated redox Pd/CZO samples, even though it was reduced prior to analysis. The ability of Pd to form stable Pd^{+2} on the support surface oxide may be vital to achieving significant Pd size reduction when inside the conditions of the Pd redispersion zone.

5. Conclusions

The trends in the aging severity at 700 °C for different Pd/CZO sample aging methods for 2 h and 16 h were as follows: redox > rich-only » lean-only. Reducing conditions produced a loss in exposed Pd surface area that was consistent with SMSI effects with support CeO_2. After each aging interval, the 700 °C/2 h lean treatment applied after redox aging always increased the Pd dispersion towards the level of the lean-only aged sample, but the magnitude of Pd dispersion recovery diminished with aging duration. These results show how quickly reducing conditions (i.e., engine fuel enrichment) and highway driving catalyst temperatures can deactivate Pd/CZO, and how frequent engine fuel-cut events must be delivered. We have shown the importance of maintaining Pd below 8.8 nm for efficient and rapid redispersion, and based on the increasing difficulty of achieving the same result for longer aging times, it is recommended that a fuel cut be performed just after 20 min of 700 °C stoichiometric (redox) operation as a practical method to maintain activity.

The approach presented here combines several methods to elucidate the Pd particle size and dispersion at different temperatures, the fraction of reducible Pd, the coverage of particles by the CZO support and the effects of various aging treatments on the effectiveness of a lean redispersion method. The good consistency of the measurements with established models for particle growth kinetics allows for estimation of the growth rates to temperatures beyond the range accessible by these methods. From these extrapolations, we are able to further estimate the effectiveness of the lean treatments to achieve redispersion and infer a recommendation for a practical engine control strategy. This approach fills a critical gap in catalyst aging measurements and allows for more confidence in applying engine control methods to preserve catalyst performance over the life of the vehicle.

Acknowledgements

The authors gratefully acknowledge the following sources of funding for this study: Ford University Research Program (URP), NSF GOALI grant # CBET-1159279 and NSF grant # DMR-9871177.

References

[1] J. Kašpar, P. Fornasiero, N. Hickey, Automotive catalytic converters: current status and some perspectives, Catal. Today 77 (2003) 419–449.
[2] M. Shelef, R. McCabe, Twenty-five years after introduction of automotive catalysts: what next? Catal. Today 62 (2000) 35–50.
[3] A. Datye, Q. Xu, K. Kharas, J. McCarty, Particle size distributions in heterogeneous catalysts: what do they tell us about the sintering mechanism? Catal. Today 111 (2006) 59–67.
[4] R. Goeke, A. Datye, Model oxide supports for studies of catalyst sintering at elevated temperatures, Top. Catal. 46 (2007) 3–9.
[5] L. Martín, J. Arranz, O. Prieto, R. Trujillano, M. Holgado, M. Galán, V. Rives, Simulation three-way catalyst ageing analysis of two conventional catalyst, Appl. Catal. B: Environ. 44 (2003) 41–52.
[6] C. Bartholomew, Mechanisms of catalyst deactivation, Appl. Catal. A: Gen. 212 (2001) 17–60.
[7] R. McCabe, R. Useman, Characterization of Pd-based automotive catalysts, Stud. Surf. Sci. Catal. 101 (1996) 355–368.
[8] Q. Xu, K.C. Kharas, B.J. Croley, A.K. Datye, The sintering of supported Pd automotive catalysts, ChemCatChem 3 (2011) 1004–1014.
[9] Z. Han, J. Wang, H. Yan, J. Fan, Performance of dynamic oxygen storage capacity, water–gas shift and steam reforming reactions over Pd-only three-way catalysts, Catal. Today 158 (2010) 481–489.
[10] H. Vidal, J. Kašpar, M. Pijolat, G. Colon, S. Bernal, A. Cordón, V. Perrichon, F. Fally, Redox behavior of CeO_2–ZrO_2 mixed oxides II. Influence of redox treatments on low surface area catalysts, Appl. Catal. B: Environ. 30 (2001) 75–85.
[11] E. Mamontov, T. Egami, R. Brezny, M. Koranne, S. Tyagi, Lattice defects and oxygen storage capacity of nanocrystalline ceria and ceria–zirconia, J. Phys. Chem. B 104 (2000) 11110–11116.
[12] T. Bunluesin, R. Gorte, G. Graham, Studies of the water-gas-shift reaction on ceria-supported Pt, Pd, and Rh: implications for oxygen-storage properties, Appl. Catal. B: Environ. 15 (1998) 107–114.
[13] R.J. Gorte, Ceria in catalysis: from automotive applications to the water–gas shift reaction, AIChE J. 56 (5) (2010) 1126–1135.
[14] M. Zhao, M. Shen, J. Wang, W. Wang, Influence of Pd morphology and support surface area on redox ability of $Pd/Ce_{0.67}Zr_{0.33}O_2$ under CO-He pulse and transient CO–O_2 measurements, Ind. Eng. Chem. Res. 46 (2007) 7883–7890.
[15] L. Kępiński, M. Wolcyrz, J. Okal, Effect of chlorine on microstructure and activity of Pd/CeO_2 catalysts, J. Chem. Soc. Faraday Trans. 91 (1995) 507–515.
[16] G. Graham, A. Shigapov, Revised model of strain in ceria–zirconia encapsulated precious-metal particles, Catal. Lett. 81 (2002) 253–258.
[17] G. Graham, A. O'Neill, A. Chen, Pd encapsulation in automotive exhaust-gas catalysts, Appl. Catal. A: Gen. 252 (2003) 437–445.
[18] N. Hickey, P. Fornasiero, R. Di Monte, J. Kašpar, J.R. González-Velasco, M.A. Gutiérrez-Ortiz, M.P. González-Marcos, J.M. Gatica, S. Bernal, Reactivation of aged model $Pd/Ce_{0.68}Zr_{0.32}O_2$ three-way catalyst by high temperature oxidising treatment, Chem. Commun. 1 (2004) 196–197.
[19] X. Chen, Y. Cheng, C.Y. Seo, J.W. Schwank, R.W. McCabe, Aging, re-dispersion, and catalytic oxidation characteristics of model Pd/Al_2O_3 automotive three-way catalysts, Appl. Catal. B: Environ. 163 (2015) 499–509.
[20] J.J. Chen, E. Ruckenstein, Role of interfacial phenomena in the behavior of alumina-supported palladium crystallites in oxygen, J. Phys. Chem. 85 (1981) 1606–1612.

[21] N.M. Rodriguez, S.G. Oh, R.A. Dalla-Betta, R.T.K. Baker, In-situ electron microscopy studies of palladium supported on Al_2O_3, SiO_2, and ZrO_2 in oxygen, J. Catal. 157 (1995) 676–686.
[22] E. Ruckenstein, J.J. Chen, Wetting phenomena during alternating heating in O_2 and H_2 of supported metal crystallites, J. Colloid Interface Sci. 86 (1982) 1–11.
[23] H. Lieske, J. Völter, Pd redispersion by spreading of PdO in O_2 treated Pd/Al_2O_3, J. Phys. Chem. 89 (1985) 1841–1842.
[24] T.R. Johns, R.S. Goeke, V. Ashbacher, P.C. Thüne, J.W. Niemantsverdriet, B. Kiefer, C.H. Kim, M.P. Balogh, A.K. Datye, Relating adatom emission to improved durability of Pt–Pd diesel oxidation catalysts, J. Catal. 328 (2015) 151–164.
[25] R.J. Farrauto, J.K. Lampert, M.C. Hobson, E.M. Waterman, Thermal decomposition and reformation of PdO catalysts; support effects, Appl. Catal. B: Environ. 6 (1995) 263–270.
[26] M. Peuckert, XPS study on surface and bulk palladium oxide, its thermal stability, and a comparison with other noble metal oxides, J. Phys. Chem. 89 (1985) 2481–2486.
[27] J. Nunan, J. Lupescu, G. Denison, D. Ball, D. Moser, HC traps for gasoline and ethanol applications, SAE Int. J. Fuels Lubrs. 6 (2) (2013) 430–449.
[28] M.A. Newton, C. Belver-Coldeira, A. Martínez-Arias, M. Fernández-García, Oxidationless promotion of rapid palladium redispersion by oxygen during redox $CO/(NO+O_2)$ cycling, Angew. Chem. Int. Ed. 46 (2007) 8629–8631.
[29] J.A. Lupescu, J.W. Schwank, K.A. Dahlberg, C.Y. Seo, G.B. Fisher, S.L. Peczonczyk, K. Rhodes, M.J. Jagner, L.P. Haack, Pd model catalysts: effect of aging environment and lean redispersion, Appl. Catal. B: Environ. 183 (2016) 343–360.
[30] A. Badri, C. Binet, J.-C. Lavalley, Metal-support interaction in Pd/CeO2 catalysis Part 2.—Ceria textural effects, J. Chem. Soc. Faraday Trans. 92 (9) (1996) 1603–1608.
[31] H.P. Sun, X.P. Pan, G.W. Graham, H.-W. Jen, R.W. McCabe, S. Thevuthasan, C.H.F. Peden, Partial encapsulation of Pd particles by reduced ceria–zirconia, Appl. Phys. Lett. 87 (2005) 201915.
[32] L. Kępiński, M. Wolcyrz, Microstructure of Pd/CeO_2 catalyst: effect of high temperature reduction in hydrogen, Appl. Catal. A. Gen. 150 (1997) 197–220.
[33] T.P. Bebee, J.T. Yeates, Spectroscopic detection of (1 1 1) facets on supported Pd crystallites: site blocking by ethyldyne on Pd/Al_2O_3, Surf. Sci. Lett. 173 (1986) L606–L612.
[34] R.F. Hicks, A.T. Bell, Effects of metal-support interactions on the hydrogenation of CO over Pd/SiO_2 and Pd/La_2O_3, J. Catal. 90 (1984) 205–220.
[35] D. Briggs, M.P. Seah, Practical Surface Sci. Analysis by Auger and X-ray Photoelectron Spectroscopy, John Wiley& Sons, New York, 1984.
[36] J.E. Benson, H.S. Hwang, M. Boudart, Hydrogen–oxygen titration method for the measurement of supported palladium surface areas, J. Catal 30 (1973) 146–153.
[37] V. Ragaini, R. Giannantonio, P. Magni, L. Lucarelli, G. Leofanti, DIspersion measurement by the single introduction method coupled with the back-sorption procedure: a chemisorption and tpd study of the different chemisorbed hydrogen species II. Pd on alumina, J. Catal. 146 (1994) 116–125.
[38] T. Takeguchi, S. Manabe, R. Kikuchi, K. Eguchi, T. Kanazawa, S. Matsumoto, W. Ueda, Determination of dispersion of precious metals on CeO_2-containing supports, Appl. Catal. A: Gen. 293 (2005) 91–96.
[39] A.L. Patterson, The Scherrer formula for X-ray particle size determination, Phys. Rev. 56 (1939) 978–982.
[40] S. Colussi, A. Trovarelli, E. Vesselli, A. Baraldi, G. Comelli, G. Groppi, J. Llorca, Structure and morphology of Pd/Al_2O_3 and $Pd/CeO_2/Al_2O_3$ combustion catalysts in Pd–PdO transformation hysteresis, Appl. Catal. A: Gen. 390 (2010) 1–10.
[41] A. Baylet, S. Royer, P. Marécot, J. Tatibouët, D. Duprez, Effect of Pd precursor salt on the activity and stability of Pd-doped hexaaluminate catalysts for the CH_4 catalytic combustion, Appl. Catal. B: Environ. 81 (2008) 88–96.
[42] R.F. Hicks, Q.-J. Yen, A.T. Bell, Effects of metal-support interactions on the chemisorption of H_2 and CO on Pd/SiO_2 and Pd/La_2O_3, J. Catal. 89 (1984) 498–510.
[43] J.S. Rieck, A.T. Bell, Studies of the interactions of H_2 and CO with Pd/SiO_2 promoted with La_2O_3, CeO_2 Pr_6O_{11}, Nd_2O_3, and Sm_2O_3, J. Catal. 99 (1986) 278–292.
[44] C.R. Adams, H.A. Benesi, R.M. Curtis, R.G. Meisenheimer, Particle size determination of supported catalytic metals: platinum on silica gel, J. Catal. 1 (1962) 336–344.
[45] J.K. Plischke, M.A. Vannice, Effect of pretreatment on the adsorption properties of silver crystallites, Appl. Catal. 42 (1988) 255–283.
[46] R.T.K. Baker, E.B. Prestridge, G.B. McVicker, The interaction of palladium with alumina and titanium oxide supports, J. Catal. 89 (1984) 422–432.
[47] F.M. Dautzenberg, H.B.M. Wolters, State of dispersion of platinum in alumina-supported catalysts, J. Catal. 51 (1978) 26–39.
[48] L. Yang, X. Yang, S. Lin, R. Zhou, Insights into the role of a structural promoter (Ba) in three-way catalyst Pd/CeO2–ZrO2 using in situ DRIFTS, Catal. Sci. Technol. 5 (2015) 2688–2695.
[49] K. Tanikawa, C. Egawa, Effect of barium addition on CO oxidation activity of palladium catalysts, Appl. Catal. A: Gen. 403 (2011) 12–17.
[50] M. Zhao, X. Li, L. Zhang, C. Zhang, M. Gong, Y. Chen, Catalytic decomposition of methanol to carbon monoxide and hydrogen over palladium supported on $Ce_{0.65}Zr_{0.30}La_{0.05}O_2$ and La–Al_2O_3, Catal. Today 175 (2011) 430–434.
[51] M.Y. Smirnov, G.W. Graham, Pd oxidation under UHV in a model Pd/ceria–zirconia catalyst, Catal. Lett. 72 (2001) 39–44.
[52] J.Z. Shyu, K. Otto, W.L.H. Watkins, G.W. Graham, R.K. Belitz, H.S. Gandhi, Characterization of Pd γ-alumina catalysts containing ceria, J. Catal. 114 (1988) 23–33.
[53] M. Alexandrou, R.M. Nix, The growth, structure and stability of ceria overlayers on Pd(1 1 1), Surf. Sci. 321 (1994) 47–57.
[54] A. Holmgren, B. Anderson, D. Duprez, Interactions of CO with Pt/ceria catalysts, Appl. Catal. B: Environ. 22 (1999) 215–230.
[55] G.N. Vayssilov, M. Mihaylov, P. St, K.I. Petkov, K.M.N. Hadjiivanov, Reassignment of the vibrational Spectra of carbonates, formates, and related surface species on ceria: a combined density functional and infrared spectroscopy investigation, J. Phys. Chem. C 115 (2011) 23435–23454.
[56] N.B. Colthup, Spectra-structure correlations in the infra-red region, J. Opt. Soc. Am. 40 (1950) 397–400.
[57] F.M. Hoffmann, Infrared reflection–absorption spectroscopy of adsorbed molecules, Surf. Sci. Rep. 3 (1983) 107–192.
[58] J. Szanyi, W.K. Kuhn, D.W. Goodman, CO adsorption on Pd(111) and Pd(100): low and high pressure correlations, J. Vac. Sci. Technol. A 11 (1993) 1969–1974.
[59] S. Bertarione, D. Scarano, A. Zecchina, V. Johánek, J. Hoffmann, S. Schauermann, M.M. Frank, J. Libuda, G. Rupprechter, H.-J. Freund, Surface reactivity of Pd nanoparticles supported on polycrystalline substrates as compared to thin film model catalysts: infrared study of CO adsorption, J. Phys. Chem. B 108 (2004) 3603–3613.
[60] M. Avrami, Kinetics of phase change. I general theory, J. Chem. Phys. 7 (1939) 1103–1112.
[61] M. Avrami, Kinetics of phase change. II transformation-time relations for random distribution of nuclei, J. Chem. Phys. 8 (1940) 212–224.
[62] T. Matsui, T. Hoshikawa, K. Naito, Oxidation of simulated fission-produced noble metals and alloy, Solid State Ionics 40/41 (1990) 996–999.
[63] E.T. Peterson, A.T. DeLaRiva, S. Lin, R.S. Johnson, H. Guo, J.T. Miller, J.H. Kwak, C.H.F. Peden, B. Kiefer, L.F. Allard, F.H. Ribeiro, A.K. Datye, Low-temperature carbon monoxide oxidation catalysed by regenerable atomically dispersed palladium on alumina, Nat. Commun. 5 (2014) 4885.